Journal for ImmunoTherapy of Cancer

CD22 CAR-T cells secreting CD19 T-cell engagers for improved control of B-cell acute lymphoblastic leukemia progression

Javier Arroyo-Ródenas ,[1,2,3] Aida Falgas,[4,5] Laura Díez-Alonso ,[1,2,3] Alba Martinez-Moreno,[4,5] Heleia Roca-Ho,[4,5] Francisco J. Gil-Etayo,[1] Alba Pérez-Pons,[6,7,8,9] Óscar Aguilar-Sopeña,[10,11] Miriam Velasco-Sidro,[1,2,3] Marina Gómez-Rosel,[1,2,3] Beatriz Jiménez-Matías ,[1,2] Guillermo Muñoz-Sánchez,[12] Yedra Pacheco,[1,2,3] Clara Bravo-Martín,[10,11] Ángel Ramírez-Fernández,[1,2,3] Anaïs Jiménez-Reinoso,[1,2,3] Europa Azucena González-Navarro,[12] Manel Juan ,[5,12] Alberto Orfao,[6,7,8,9] Belén Blanco,[1,2,3] Pedro Roda-Navarro,[10,11] Clara Bueno,[4,5,8] Pablo Menéndez,[4,5,8,13,14,15] Luis Álvarez-Vallina [1,2,3,16,17]

To cite: Arroyo-Ródenas J, Falgas A, Díez-Alonso L, *et al*. CD22 CAR-T cells secreting CD19 T-cell engagers for improved control of B-cell acute lymphoblastic leukemia progression. *Journal for ImmunoTherapy of Cancer* 2025;**13**:e009048. doi:10.1136/jitc-2024-009048

JA-R and AF are joint first authors.

Accepted 07 April 2025

For numbered affiliations see end of article.

Correspondence to
Dr Luis Álvarez-Vallina; lalvarezv@ext.cnio.es

Dr Clara Bueno; cbueno@carrerasresearch.org

Dr Pablo Menéndez; pmenendez@carrerasresearch.org

ABSTRACT

Background CD19-directed cancer immunotherapies, based on engineered T cells bearing chimeric antigen receptors (CARs, CAR-T cells) or the systemic administration of bispecific T cell-engaging (TCE) antibodies, have shown impressive clinical responses in relapsed/refractory B-cell acute lymphoblastic leukemia (B-ALL). However, more than half of patients relapse after CAR-T or TCE therapy, with antigen escape or lineage switching accounting for one-third of disease recurrences. To minimize tumor escape, dual-targeting CAR-T cell therapies simultaneously targeting CD19 and CD22 have been developed and validated both preclinically and clinically.

Methods We have generated the first dual-targeting strategy for B-cell malignancies based on CD22 CAR-T cells secreting an anti-CD19 TCE antibody (CAR-STAb-T) and conducted a comprehensive preclinical characterization comparing its therapeutic potential in B-ALL with that of previously validated dual-targeting CD19/CD22 tandem CAR cells (TanCAR-T cells) and co-administration of two single-targeting CD19 and CD22 CAR-T cells (pooled CAR-T cells).

Results We demonstrate that CAR-STAb-T cells efficiently redirect bystander T cells, resulting in higher cytotoxicity of B-ALL cells than dual-targeting CAR-T cells at limiting effector:target ratios. Furthermore, when antigen loss was replicated in a heterogeneous B-ALL cell model, CAR-STAb T cells induced more potent and effective cytotoxic responses than dual-targeting CAR-T cells in both short- and long-term co-culture assays, reducing the risk of CD19-positive leukemia escape. In vivo, CAR-STAb-T cells also controlled leukemia progression more efficiently than dual-targeting CAR-T cells in patient-derived xenograft mouse models under T cell-limiting conditions.

Conclusions CD22 CAR-T cells secreting CD19 T-cell engagers show an enhanced control of B-ALL progression compared with CD19/CD22 dual CAR-based therapies, supporting their potential for clinical testing.

WHAT IS ALREADY KNOWN ON THIS TOPIC

⇒ A significant proportion of patients with B-cell acute lymphoblastic leukemia (B-ALL) relapse after initial response to anti-CD19 chimeric antigen receptor (CAR)-T or T cell-engagers (TCEs). Dual-targeting therapies have emerged as an alternative to prevent antigen loss and minimize tumor escape.

WHAT THIS STUDY ADDS

⇒ Dual-targeting CD22 CAR-T cells secreting anti-CD19 TCEs efficiently recruit bystander non-transduced T cells, inducing more potent and rapid cytotoxic responses than dual CD19/CD22 CAR-T cell therapies both in vitro and in vivo and reducing the risk of CD19-positive leukemia progression.

HOW THIS STUDY MIGHT AFFECT RESEARCH, PRACTICE OR POLICY

⇒ The dual-targeting CAR-secreting T cell-engaging antibodies represent a promising alternative approach to single and dual CAR-T cell therapies for the treatment of relapsed/refractory B-ALL, encouraging clinical development.

INTRODUCTION

CD19-specific cancer immunotherapies, based on either the adoptive transfer of engineered T cells bearing chimeric antigen receptors (CARs) or the systemic administration of bispecific T cell-engagers (TCEs), have shown impressive clinical responses in relapsed/refractory (R/R) B-cell acute lymphoblastic leukemia (B-ALL).[1–7] However, around 50% of treated patients still show disease recurrence within 1 year of

treatment,[8] with antigen loss being responsible for a large proportion of these relapses.[9–11] Immune escape[12–14] and phenotypic escape[15 16] are the main mechanisms underlying CD19-negative (CD19^{neg}) relapse, especially when single-antigen targeting therapies are used. Immune and phenotypic escape, coupled to intrinsic tumor heterogeneity, may trigger the selection and proliferation of CD19^{neg} subpopulations, leading to tumor escape.[17] In this context, the sequential administration of CD22-specific CAR-T cells has proven clinical benefit in both CD19^{pos} and CD19^{neg} patients who were refractory or relapsed after CD19-specific CAR-T therapy.[18 19] However, leukemia still progresses in these patients due to the emergence of CD22^{neg} or CD22^{low} leukemia cells.[18]

To prevent antigen loss after administration of single-targeting CAR-T cells and minimize tumor escape, strategies simultaneously targeting CD19 and CD22 have been developed and validated in both preclinical models[18 20 21] and clinical trials.[22 23] Several dual CD19/CD22 targeting strategies have been implemented: (1) co-administration of two different single-targeting CAR-T cell products, (2) T-cell co-transduction with two different single-targeting CAR vectors, (3) T-cell transduction with a single bicistronic vector encoding both single-targeting CARs, and (4) linking two binding domains in a tandem CAR (TanCAR) construct.[24 25] Despite their potential to prevent antigenic loss, these strategies have several limitations.[23 26] On the one hand, co-transduction may yield a low proportion of T cells expressing both CARs, while co-infusion of two monospecific CAR-T cells might lead to expansion and dominance of one population over the other, in addition to the associated increase in cost and regulatory requirements.[20] Regarding the design of bispecific CD19/CD22 TanCARs, some aspects seem to be critical to achieve adequate CD22 binding capacity,[20] the optimal distance between the CAR binding domain and the targeted epitope being decisive for the establishment of efficient immunological synapses (IS).[27–31] However, due to the membrane proximal positioning of the CD19 binding domain, the anti-CD22 single-chain variable fragment (scFv) antibody is usually relegated to a less favorable position where the increased distance between the CD22-binding epitope and the membrane, coupled with potential steric hindrance issues, may compromise the ability to transmit proper activation signals.[32] As a consequence, reduced CD22-specific cytotoxicity has been reported for CD19/CD22 TanCAR T cells compared with monospecific CD22 CAR-T cells.[20 23] To date, clinical outcomes with dual-targeting CAR-T cells in B-cell malignancies have generally been comparable to those reported with single-targeting CD19 CAR-T cells.[23] Therefore, novel approaches that integrate diverse mechanisms to target multiple antigens may be essential for advancing the successful treatment of these tumors.

The in vivo secretion of TCE antibodies by genetically engineered (STAb) T cells is an emerging strategy to achieve sustained serum TCE concentrations and persistence of adoptively transferred T cells.[26 33–37] In addition, unlike CAR-T, STAb-T cells can recruit unmodified bystander T cells and induce the formation of canonical IS,[38] resulting in enhanced antitumor responses.[36 37 39] Currently, several STAb-T therapies have shown promising results in both B-cell[36 40 41] and T-cell[37] hematological malignancies and in multiple myeloma.[39] The combination of CAR-T and STAb-T could address the inability of CAR-T cells to recruit bystander T lymphocytes and the lack of a second activation signal associated with TCE, providing a synergistic strategy to maximize the efficacy, strength and durability of clinical responses.[8 42] Combining these two distinct mechanisms of action into a unique dual-targeting strategy may also circumvent the complexity and steric limitations of TanCAR-T cells, in addition to overcoming antigen-negative relapses associated with single-targeting immunotherapies.[24 42 43] Dual-targeting strategies combining a CAR and a TCE have only been reported to date in solid tumors[44–50] and, more recently, in myeloid leukemias.[51 52] Here, we have developed the first dual-targeting CAR-STAb-T strategy for B-cell malignancies, CD22-targeted CAR-T cells secreting a CD19×CD3 TCE, and demonstrated that CAR-STAb-T cells are more effective than dual-targeting CAR-based strategies (i.e., CD19/CD22 TanCAR-T cells or pooled CD19/CD22 CAR-T cells) in several cutting-edge in vitro and in vivo models of B-ALL.

METHODS

T-cell transduction

Peripheral blood mononuclear cells were isolated from peripheral blood (PB) of volunteer healthy donors by density gradient centrifugation using Lymphoprep (Axis-Shield, Oslo, Norway). Cells were plate-coated and activated with 1 µg/mL anti-CD3 (OKT3 clone, BD Biosciences, San Jose, California, USA) and 1 µg/mL anti-CD28 (CD28.2 clone, BD Biosciences) monoclonal antibodies for 2 days and transduced at multiplicity of infection (MOI) 10 with CD22-CAR-, CD19-TCE-, CD19-CAR-, CD19-CD22-TanCAR- or CD22-CAR-CD19-TCE-encoding lentiviruses in the presence of 10 ng/mL interleukin (IL)-7 and 10 ng/mL IL-15 (both from Miltenyi Biotec, Bergisch Gladbach, Germany). As negative controls, non-transduced primary T cells (NT-T) were used. Alternatively, T cells were activated with anti-CD3/CD28 magnetic beads (Thermo Fisher) for 3 days. A 6–10 days expansion period was carried out before conducting experiments. In addition, Jurkat T cells (1×10^5) were transduced with the abovementioned lentiviruses at MOI of 5 for CD22-CAR, CD19-TCE or CD19-CAR constructs and 10 for CD19-CD22-TanCAR- or CD22-CAR-CD19-TCE-encoding lentiviruses. Non-transduced Jurkat T cells (J-NT-T) were used as negative controls. Cells were cultured in Roswell Park Memorial Institute-1640 supplemented with 2 mM L-glutamine, heat-inactivated 10% fetal bovine serum and antibiotics.

Cytotoxicity assays

Activated transduced T (A-T) cells (CAR-T22, STAb-T19, CAR-T19, TanCAR-T or CAR-STAb-T) were co-cultured

with luciferase-expressing tumor target cells (NALM6^{Luc}, SEM^{Luc} or K562^{Luc}) at the indicated effector:target (E:T) ratios. For bystander cytotoxicity assays, A-T cells were co-cultured with or without freshly isolated T cells (non-activated T cells, NA-T) from the same healthy donor and luciferase-expressing target cells (NALM6^{Luc}) at the indicated A-T:T ratios, keeping a constant 1:1 E:T ratio. For cytotoxic studies in non-contacting transwell systems, polycarbonate filter inserts (4.26 mm diameter) with 0.4 µm pores (Corning, Kennebunk, Maine, USA) were used. In these experiments, 5×10^4 NALM6^{Luc} target cells were plated on bottom wells and A-T cells were added to the transwell inserts at the indicated A-T:T ratios. Increasing numbers of NA-T cells were also plated in the bottom wells to maintain a constant 1:1 E:T ratio. After 48 hours, supernatants were collected and stored at −20°C for further cytokine secretion analysis, and D-luciferin (Promega, Madison, Wisconsin, USA) was added to cells to a final concentration of 20 µg/mL before bioluminescence quantification in relative light units using a Victor luminometer (PerkinElmer, Waltham, Massachusetts, USA). The value for spontaneous lysis was obtained by incubating the target cells with NT-T effector cells. Per cent-specific cytotoxicity was calculated using the formula: 100 − ((bioluminescence of each sample × 100) / mean bioluminescence of NT-cells). Specific lysis was established as 100% of cell viability.

Mouse xenograft models

7–12-week-old non-obese diabetic Cg-Prkdcscid Il2rgtm1Wjl/SzJ (NSG) mice (The Jackson Laboratory, Bar Harbor, Maine, USA) were bred and housed under pathogen-free conditions. For the in vivo experiments with B-ALL cell lines, NSG mice were intravenously infused with 1×10^6 SEM^{Luc} WT or a mixture of 2.5×10^5 SEM^{Luc} cells (33% SEM^{WT}, 33% CD19^{KO} and 33% CD22^{KO}). After 5 days, mice were intravenously injected with $4–5\times10^6$ T cells (NT, TanCAR-T, CAR-STAb-T or a 1:1 mix of CAR-T19 and CAR-T22). For the in vivo experiments using patient-derived xenograft (PDX) models, NSG mice were sublethally irradiated (2 Gy) and intravenously infused with 1×10^6 CD19^{pos} CD22^{pos} B-ALL blasts.

Leukemic engraftment was monitored by weekly analysis of PB. When leukemic cells were detectable in PB, mice were homogenously allocated to three different groups and received 3×10^6 NT-T, TanCAR-T or CAR-STAb-T cells. Tumor burden (HLA-ABC^{pos} CD45^{neg}) and effector T-cell persistence (HLA-ABC^{pos} CD45^{pos}) were monitored weekly by PB flow cytometry. SEM^{Luc} progression was also evaluated weekly by bioluminescence signal (BLI, total photons) as previously described[36] using the Xenogen IVIS Lumina II imaging system (Caliper Life Sciences). Animals were euthanized when they had lost >20% of their body weight, exhibited signs of disease or reached the BLI emission established at the beginning of the experiment. PB, bone marrow (BM), brain, plasma and cerebrospinal fluid (CSF) samples were collected at the end of the experiment for flow cytometry analysis or cytokine determination. Plasma was collected by intracardiac puncture after the blood centrifugation (1,500×g, 10 min, 4°C), whereas the CSF was collected from the cisterna magna following the previous instructions.[53]

Statistical analysis

Statistical tests indicated in figure legends and data processing were performed using GraphPad Prism V.8 (GraphPad Prism Software, La Jolla, California, USA). Significant differences were determined by one-way or two-way analysis of variance followed by Tukey's multiple comparisons post hoc test, or an unpaired Student's t-test. Significance was considered only when p values were <0.05 and is defined as follows: *p<0.05; **p<0.01; ***p<0.001, ****p<0.0001). Data are presented as the mean±SEM and n represents the total number of technical and biological replicates performed.

RESULTS

Generation and characterization of CAR-STAb-T cells

In this study, a bispecific CAR-STAb construct was developed from previously validated second-generation anti-CD22 (hCD22.7) 4-1BB-CD3ζ CAR[31] and anti-CD19 (A3B1)×CD3 (OKT3) TCE (CD19-TCE)[36] (online supplemental figure S1a,b). Both sequences were cloned into a 2A-based tricistronic lentiviral vector under the control of the EF1α promoter (pCCL-CD22-CAR-F2A-CD19-TCE-T2A-EGFP) (online supplemental figure S1c). The construct was designed to target each individual antigen with a different mechanism of action, to address potential steric-hindrance-associated issues (figure 1a). The previously characterized bispecific CD22/CD19 tandem CAR,[21] containing the same CD19 and CD22 scFv domains as the CAR-STAb construct, was used as a control (online supplemental figure S1d). Jurkat T cells were successfully transduced with lentiviral particles encoding single-targeted CD22 or CD19 constructs (online supplemental figure S1a,b), to generate J-CAR-T22 and J-STAb-T19 cells, or dual-targeted CD22/CD19 constructs (online supplemental figure S1c,d), to generate J-TanCAR-T and J-CAR-STAb-T cells. Transduction efficiency, measured by CD22-CAR expression on the cell surface of J-CAR-T22, J-TanCAR-T and J-CAR-STAb-T cells or intracellular CD19-TCE on J-STAb-T19 and J-CAR-STAb-T cells, correlated with the expression of EGFP and tdTO reporter genes (online supplemental figure S2a). CD19-TCE was secreted by J-CAR-STAb-T cells, with a molecular weight of 55 kDa, although at lower levels than observed in J-STAb-T19 cells (figure 1b). A reduction in TCE secretion in the context of a bicistronic construct has been previously reported by other authors.[44] The secreted CD19-TCE specifically recognized plastic-immobilized human CD19-Fc fusion protein (CD19-Fc, online supplemental figure S2b) and CD19 expressed on the cell surface (online supplemental figure S2c).

To study target-specific activation, transduced Jurkat cells were co-cultured in direct cell–cell contact systems

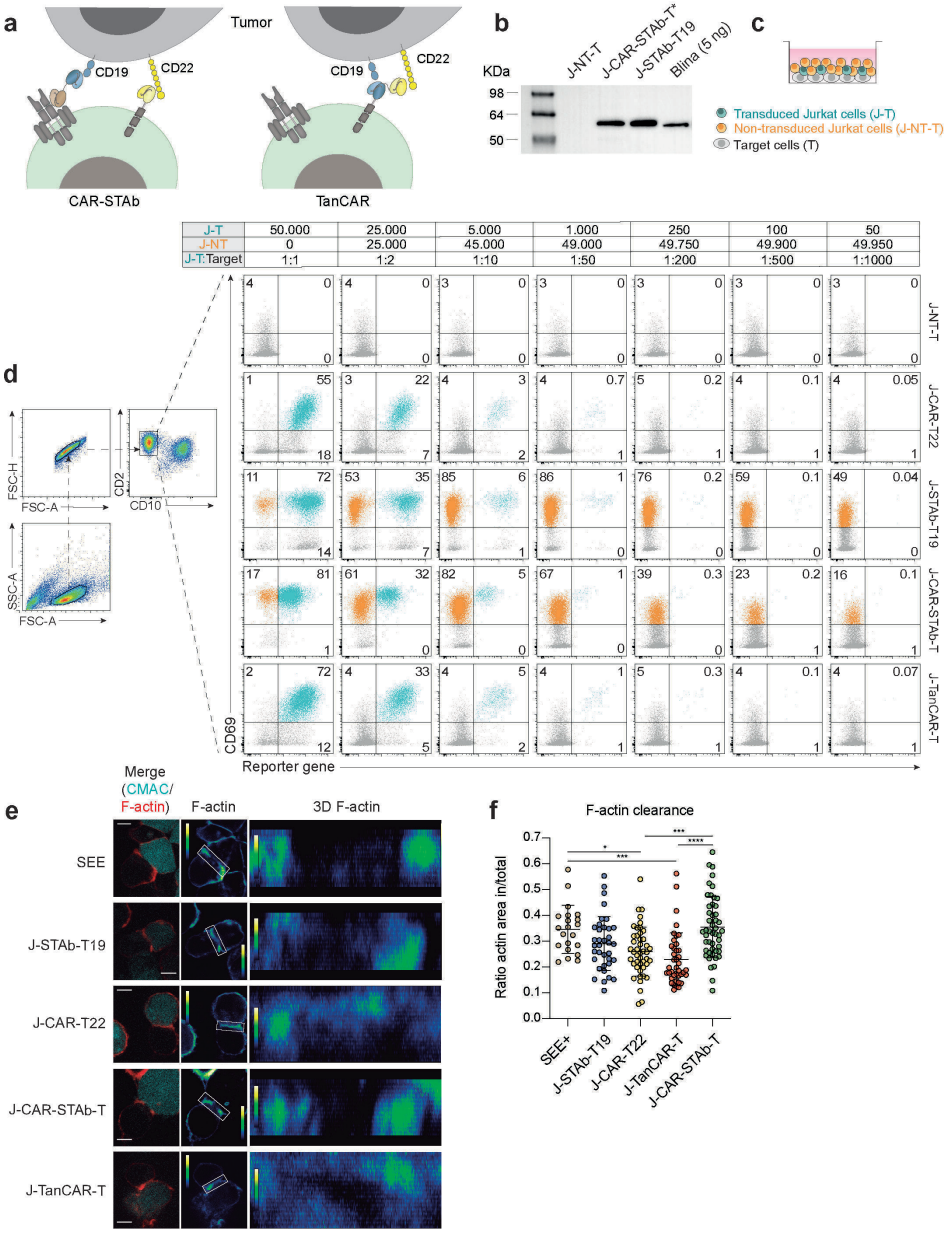

Figure 1 Comparative in vitro study of engineered STAb-19, CAR-22, TanCAR and CAR-STAb Jurkat (J) cells. (a) Schematic representation of the molecular interactions between targeted antigens and CAR or CAR and TCE in the TanCAR and CAR-STAb strategies, respectively. (b) Western blot analysis of CD19-TCE secretion in supernatants from J-CAR-STAb-T (10 times concentrated) and J-STAb-19T cells (net). Samples were subjected to SDS-PAGE and blotting with anti-His-tag antibody. (c) Schematic representation of direct contact co-culture systems to study the specific activation of J-NT-T, J-STAb-T19, J-CAR-T22, J-TanCAR-T and J-CAR-STAb-T cells against a panel of SEM cells genetically engineered using CRISPR-Cas9 technology to selectively silence the expression of one and/or two of the target antigens. (d) Recruitment and activation of transduced (teal) and non-transduced (orange) Jurkat cells cultured with Raji cells at decreasing J:T ratios. One of three independent experiments measuring CD69 by flow cytometry is shown (n=3). Percentages of activated ($CD69^{pos}$) Jurkat cells are indicated. (e) Topology of the IS induced by J-NT-T, J-STAb-19T, J-CAR-22T, J-TanCAR-T and J-CAR-STAb-T cells. Representative Jurkat/Raji cell conjugates are shown. Conjugates of Jurkat and SEE-loaded Raji cells are used to show the organization of actin at a canonical IS. F-actin distribution to the IS of a confocal section is displayed in pseudocolor. Merged image of F-actin in red and CMAC in cyan is shown for cell identification purposes. Scale bar corresponds to 5 µm. The surface interface of the interaction (pointed by a white square) obtained by 3D-confocal microscopy is shown for F-actin as pseudocolor. The calibration bar of the pseudocolor is indicated. (f) Graph showing F-actin clearance calculated from 3D reconstructions obtained at the IS. Actin clearance value from each individual dot corresponds to the ratio between the central actin cleared area and the total actin area of the 3D IS reconstruction. Each dot represents the value of individual Jurkat/Raji interactions obtained from n=2 independent experiments. Samples were compared by a one-way analysis of variance with a Tukey's multiple comparison test. Blina, blinatumomab; CAR, chimeric antigen receptor; CMAC, CellTracker Blue; IS, immunological synapses; SEE, Staphylococcal Enterotoxin E; STAb, in situ secretion of T-cell redirecting bispecific antibodies; TanCAR, tandem CAR; TCEs, T cell-engagers; 3D, three-dimensional.

(online supplemental figure S3a) with a panel of SEM cells expressing both targeted antigens, CD19 and CD22 (SEM^{WT}), only one of them, either CD19 ($SEM\text{-}CD22^{KO}$) or CD22 ($SEM\text{-}CD19^{KO}$), or neither antigen ($SEM\text{-}CD19^{KO}/22^{KO}$) (online supplemental figure S4a). Transduced Jurkat cells were specifically activated when co-cultured with SEM cells expressing at least one of the target antigens, but CD69 levels were significantly higher in the context of CD19-TCE-mediated activation compared with CD22-CAR-mediated activation (online supplemental figure S3c). Transwell assays (online supplemental figure S3b) were used to further demonstrate that CD19-TCE-secreting Jurkat T cells (J-STAb-T19 and J-CAR-STAb-T) were able to specifically activate J-NT-T when co-cultured in the lower chamber with $CD19^{pos}$ cells (online supplemental figure S3d). To better characterize the potential to recruit bystander T cells in the presence of target Raji cells, decreasing proportions of transduced Jurkat (J-T) cells (J-STAb-T19, J-CART22, J-CAR-STAb-T and J-TanCAR) were co-cultured with increasing proportions of J-NT cells to keep the total number of effector Jurkat T cells constant (figure 1c). The results demonstrate that a very small number of CD19-TCE-secreting T cells (GFP^{+}) have the potential to recruit J-NT bystander cells (GFP^{-}). The recruitment capacity of J-STAb-T19 cells was superior to that of J-CAR-STAb-T cells and remains almost stable up to J-T:target ratios of 1:50. For J-CAR-STAb-T cells, the reduced TCE secretion translates into a lower bystander T-cell recruitment capacity but is still evident even at J-T:target ratios of 1:1,000 (figure 1d). Co-cultures with $CD19^{neg}$ $CD22^{neg}$ K562 target cells and plate-bound anti-CD3 mAb (iOKT3) were used as negative and positive controls, respectively (online supplemental figure S3e).

Next, we studied the architecture of the IS by staining for CD3ε and filamentous actin (F-actin), as markers of central and distal supramolecular activation complex, respectively. J-STAb-T19, J-CAR-T22, J-TanCAR-T and J-CAR-STAb-T cells were incubated with Raji cells for 15 min to allow the assembly of the IS. Superantigen E (Staphylococcal Enterotoxin E (SEE))-loaded Raji cells co-cultured with J-NT-T cells were used as a positive control of IS formation. Confocal microscopy images showed that all Jurkat conjugates formed IS with Raji cells, based on F-actin polarization (figure 1e). However, J-STAb-T19 and J-CAR-STAb-T cells showed similar F-actin clearance values compared with SEE T-cell receptor (TCR)-stimulated J-NT-T cells and higher than J-CAR-T22 and J-TanCAR-T cells (figure 1f). These data suggest that CD19-TCE-secreting cells better mimic canonical IS formation and actin network establishment. Interestingly, only J-STAb-T19 cells could induce CD3ε polarization to the IS in a similar way to J-NT-T cells stimulated by SEE (online supplemental figure S3f,g). This could indicate that, since CAR-mediated activation is not dependent on TCR/CD3 mobilization, J-CAR-STAb-T cells do not seem to require TCR polarization to the IS to become activated, despite having a good F-actin distribution toward the IS.

CAR-STAb-T cells induce more potent specific cytotoxicity and prevent leukemia escape in vitro more effectively than TanCAR-T cells

To study the specificity and cytotoxic potential of the CAR-STAb-T cells, primary T lymphocytes were transduced with lentiviral vectors encoding single-targeting or double-targeting constructs (online supplemental figure S1a-d). Transduction efficiencies determined by reporter gene expression (figure 2a) showed good correlation with cell surface CAR levels (online supplemental figure S5). The proportion of $CD4^{pos}$ and $CD8^{pos}$ cells and the relative distribution of memory-like T-cell subsets were similar in NT-T, STAb-T19, CAR-T19, CAR-T22, TanCAR-T and CAR-STAb-T cells (figure 2b,c). First, we studied the specificity by co-culturing transduced T cells with the panel of SEM cells at a 1:4 E:T ratio. CAR-STAb-T cells efficiently killed SEM^{WT}, $SEM\text{-}CD19^{KO}$ and $SEM\text{-}CD22^{KO}$ cells, whereas STAb-T19 and CAR-T22 cells killed SEM^{WT} cells but did not show cytotoxic activity against $SEM\text{-}CD19^{KO}$ and $SEM\text{-}CD22^{KO}$ cells, respectively (online supplemental figure S6a). No cytotoxicity was observed either when $SEM\text{-}CD19^{KO}/22^{KO}$ cells were used as targets or NT-T cells as effectors (online supplemental figure S6a). Further analysis of supernatants from STAb-19 primary T cells co-cultured with $SEM\text{-}CD22^{KO}$ cells revealed a constant release of TCE over time, which correlated with highly specific and efficient cytotoxicity (online supplemental figure S6b). CAR-STAb-T cells also showed similar cytotoxic efficacy despite lower levels of TCE secretion, which remained below detection limits throughout the experiment (online supplemental figure S6b). No cytotoxicity and lower levels of TCE were detected when effector T cells were co-cultured with $SEM\text{-}CD19^{KO}/22^{KO}$ target cells (online supplemental figure S6c). Next, TanCAR-T and CAR-STAb-T cells were co-cultured with the SEM^{Luc} cell panel at E:T ratios from 1:1 to 1:8. TanCAR-T and CAR-STAb-T cells exhibited similar cytotoxic activity at the higher ratios, but CAR-STAb-T cells were significantly more effective at 1:4 or lower E:T ratios (figure 2d). No cytotoxicity was observed when $SEM\text{-}CD19^{KO}/22^{KO}$ cells were used as targets (figure 2d). In addition, we studied the cytotoxic potential of CAR-STAb-T and TanCAR-T cells against $NALM6^{Luc}$ cells (online supplemental figure S4a) under T cell-limiting conditions, using decreasing E:T ratios. According to previous results, CAR-STAb-T cells showed significantly superior cytotoxic responses compared with TanCAR-T cells even at E:T ratios as low as 1:64 (figure 2e). Interestingly, the enhanced cytotoxicity did not correlate with increased interferon gamma (IFN-γ) secretion (figure 2f).

To further assess the impact of bystander T cells on the cytotoxic potential of CAR-STAb-T cells, we co-cultured decreasing numbers of NT-T or transduced (TanCAR-T or CAR-STAb-T) activated T (A-T) effector cells with a constant number of $NALM6^{Luc}$ target (T) cells at A-T:T ratios from 1:1 to 1:50,000. Increasing numbers of freshly isolated T cells (NA-T) from the same healthy donor were added to maintain a constant 1:1 E:T ratio. After 48 hours,

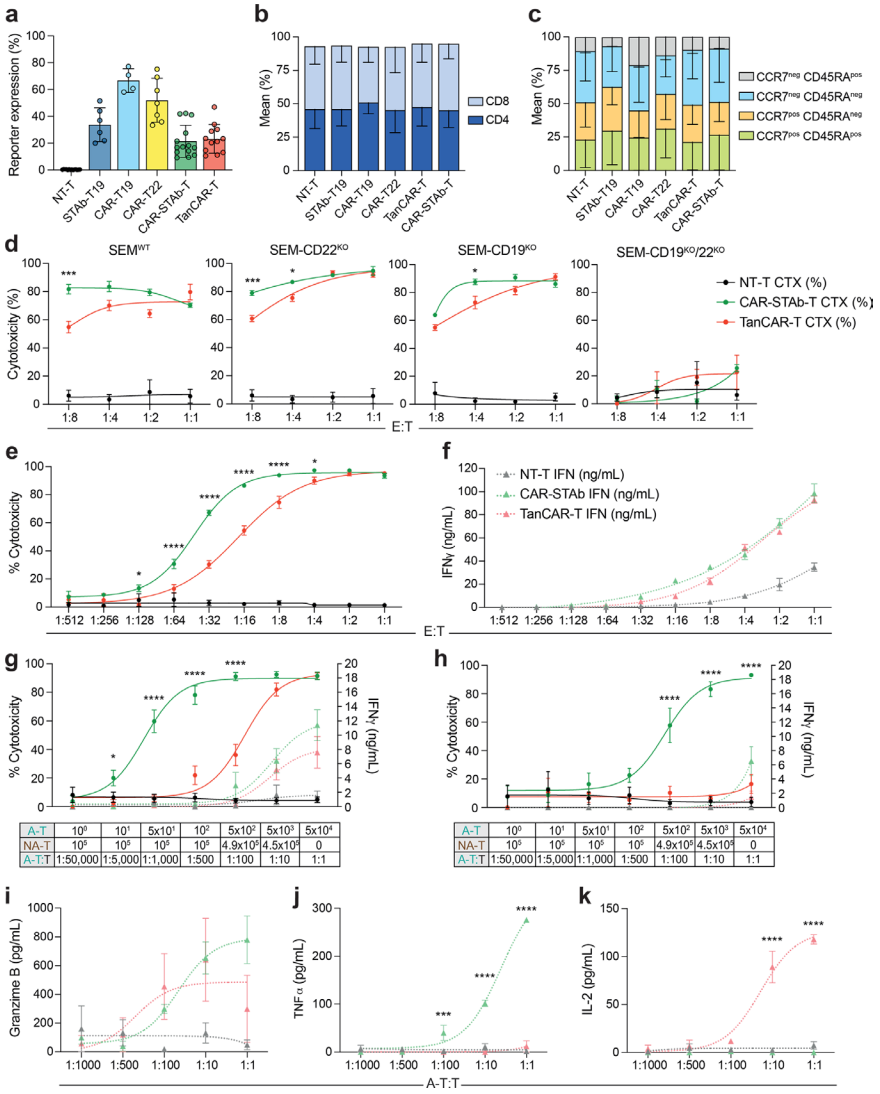

Figure 2 Comparative in vitro cytotoxicity study between CAR-STAb-T and TanCAR-T cells. (a) Transduction efficacy in primary T cells calculated by GFP for CAR-19T, CAR-22T, TanCAR-T and CAR-STAb-T cells or tdTO for STAb-19T cells. Results expressed as mean±SEM of transductions from at least four different healthy donors (n=4). (b, c) Percentages of $CD4^{pos}$ and $CD8^{pos}$ T cells (b) and percentages of $CCR7^{neg}$ $CD45RA^{neg}$, $CCR7^{neg}$ $CD45RA^{pos}$, $CCR7^{pos}$ $CD45RA^{neg}$ and $CCR7^{pos}$ $CD45RA^{pos}$ T cells (c) among NT-T, STAb-19T, CAR-22T, TanCAR-T and CAR-STAb-T cells. Results for (b, c) are mean—SEM of transductions from at least four different healthy donors (n=4). (d) Specific cytotoxicity of non-transduced (NT-T) or transduced (CAR-STAb-T or TanCAR-T) primary T cells against $CD19^{pos}/CD22^{pos}$ (SEM^{WT}), $CD19^{pos}/CD22^{neg}$ (SEM-$CD22^{KO}$), $CD19^{neg}/CD22^{pos}$ (SEM-$CD19^{KO}$) or $CD19^{neg}/CD22^{neg}$ (SEM-$CD19^{KO}/22^{KO}$) target cells at indicated E:T ratio after 48 hours. Data expressed as mean±SEM of one experiment with triplicates (n=3). Cytotoxic activity (e) and IFN-γ secretion determined by ELISA (f) of CAR-STAb-T and TanCAR-T cells co-cultured with $NALM6^{Luc}$ cells under T-cell-limiting conditions (low E:T ratios from 1:1 to 1:512). Data for (e, f) expressed as mean±SEM of two experiments with independent donors in triplicate (n=6). (g) Decreasing numbers of activated effector T (AT) cells (NT-T, CAR-STAb-T or TanCAR-T) were co-cultured with 5×10^4 $NALM6^{Luc}$ target cells. Increasing numbers of fresh isolated (NA-T) cells from the same donor (bystander T cells) were added to the culture, resulting in the indicated AT:T ratios and maintaining a constant 1:1 E:T ratio. Cytotoxicity (left Y axis) and IFN-γ secretion (right Y axis) are represented. Data expressed as mean±SEM of three experiments with independent donors in triplicate for cytotoxicity curves (n=9) and in duplicate for IFN-γ secretion curves (n=6). (h) Decreasing numbers of activated A-T cells (NT-T, CAR-STAb-T or TanCAR-T) were added to the insert wells of a non-contacting Transwell system at indicated A-T:T ratios, while 5×10^4 $NALM6^{Luc}$ cells and increasing numbers of NA-T cells were plated in the bottom wells to maintain a constant 1:1 E:T ratio. Data are mean±SEM from two experiments with independent donors, performed in triplicate for cytotoxicity curves (n=6) and duplicate for IFN-γ curves (n=4). The percentage of specific cytotoxicity was calculated after 48 hours of culture by addition of D-luciferin to detect bioluminescence (d–h) and IFN-γ secretion was determined by ELISA (f–h). (i–k) Supernatants from the bystander experiment in (g) were tested in a multiplex bead-based immunoassay for the secretion of granzyme B (i), tumor necrosis factor-α (j) and IL-2 (k). Data for (i–k) expressed as mean±SEM of one experiment performed in triplicate (n=3). Statistical significance was calculated by two-way analysis of variance test corrected with a Tukey's multiple comparisons test. CAR, chimeric antigen receptor; E:T, effector:target; IFN, interferon; STAb, in situ secretion of T-cell redirecting bispecific antibodies; TanCAR, tandem CAR.

CAR-STAb-T cells reached a cytotoxicity higher than 80% even at the 1:500 A-T:T ratio, whereas TanCAR-T cells could only reach this activity at the 1:10 A-T:T ratio (figure 2g). Similar experiments in non-contact co-culture systems were performed. In this case, NA-T cells were plated with NALM6^{Luc} cells in the bottom wells, whereas A-T cells were plated in the upper chamber of the transwell system. In contrast to NT-T and TanCAR-T cells, CAR-STAb-T cells induced 80% target cell lysis activity at an A-T:T 1:10 ratio and more than 50% at the 1:100 ratio (figure 2h). Regarding cytokine secretion, no statistical differences in IFN-γ and granzyme B levels were found, despite the enhanced cytotoxic activity shown by CAR-STAb-T cells (figure 2g,i). However, a different profile of tumor necrosis factor (TNF)-α and IL-2 secretion between CAR-STAb-T and TanCAR-T cells was observed, with increased levels of IL-2 for TanCAR-T and TNF-α for CAR-STAb-T cells at higher E:T ratios (figure 2j,k). To further investigate the ability to prevent leukemia escape, long-term cultures of CAR-STAb-T or TanCAR-T cells were established with NALM6^{Luc} cells at decreasing E:T ratios (online supplemental figure S7a). After 2 weeks, CAR-STAb-T cells prevented leukemia escape at 1:1, 1:2 and 1:4 E:T ratios, while TanCAR-T cells prevented escape only at the 1:1 ratio (online supplemental figure S7b).

CAR-STAb-T cells control CD19^{pos} CD22^{pos} B-ALL more efficiently than TanCAR-T cells in vivo

We next compared the antitumor activity of CAR-STAb-T and TanCAR-T cells under T cell-limiting conditions in vivo in NSG mice intravenously injected with 1×10^6 SEM^{Luc} WT cells homogeneously expressing CD19 and CD22 (online supplemental figure S4a), followed 4 days later by intravenous infusion of 4×10^6 T cells, where CAR-STAb^{pos} or TanCAR^{pos} cells comprised 8% of the infused T cells (3.2×10^5 cells). Leukemia progression was followed weekly by BLI, and PB, BM, brain and CSF samples were analyzed at the endpoint (figure 3a). Leukemia progressed rapidly in all mice receiving NT-T cells, while one out of three mice in the TanCAR-T group and two out of three mice injected with CAR-STAb-T cells showed clear evidence of leukemia control after 3 weeks by both bioluminescence and flow cytometry (figure 3b,c). Despite the increased T-cell expansion found in the PB and BM of TanCAR-T treated mice, no significant differences were observed in the percentage of blasts in PB, BM and brain between the TanCAR-T and CAR-STAb-T groups (figure 3d). Similarly, there were no differences among the groups in the production of the cytokines IFN-γ, IFN-β, IL-1β, IL-6 and IL-10 in both plasma and CSF samples (figure 3e).

Next, the antitumor activity of CAR-STAb-T and TanCAR-T cells in vivo was compared in a more clinically relevant PDX model under similar conditions as in the previous experiment. NSG mice were intravenously injected with 1×10^6 primary B-ALL cells homogeneously expressing CD19 and CD22 (online supplemental figure S8), followed 3 weeks later by intravenous infusion of 3×10^6 T cells, where CAR-STAb^{pos} or TanCAR^{pos} cells comprised 8% of the infused T cells (2.4×10^5 cells) (figure 3f). Leukemia progression and T-cell expansion were followed in PB and BM by flow cytometry at indicated time points (figure 3f) until week 5, when mice were euthanized due to the development of xenogeneic graft-versus-host disease. In all mice receiving NT-T cells and in two of six TanCAR-T-treated mice, leukemia progressed rapidly, whereas four of six TanCAR-T-treated and all CAR-STAb-T-treated mice showed evidence of leukemia control at week 5 (figure 3g and online supplemental figure S9). Half of the CAR-STAb-T-treated mice, but none in the NT-T or TanCAR-T groups, showed strict leukemia control with ≤1% blasts in PB during the entire experiment (figure 3g and online supplemental figure S9). Further analysis of BM at week 3 revealed complete/near-complete disease control in three out of six CAR-STAb-treated mice, while clear leukemia infiltration in BM was observed in mice receiving NT-T and TanCAR-T cells (figure 3h). In this case, the rapid and stable disease control in CAR-STAb-T cell-treated mice correlated with increased T-cell infiltration in the BM (figure 3i).

CAR-STAb-T cells control heterogeneous B-ALL more efficiently than dual-targeted CAR-T cells in vitro

To compare the in vitro cytotoxic activity of the different dual-targeting approaches in the context of a heterogeneous leukemia, we set up a mixed B-ALL model containing equal percentages of SEM^{WT}, SEM-CD19^{KO} and SEM-CD22^{KO} cells (33% SEM cell mix). Long-term co-cultures were established with effector T cells (NT-T, TanCAR-T, CAR-STAb-T or a 1:1 mixture of single-targeted CAR-T19 (A3B1) and CAR-T22 (hCD22.7) (pooled CAR-T)) and the 33% SEM target cell mix at the indicated E:T ratios (figure 4a). At day 11, leukemia cells escaped from CAR-STAb-T cells only at the 1:8 and 1:16 E:T ratios, while CAR-T and TanCAR-T cells were only able to control tumor progression at the 1:1 and 1:2 E:T ratios. Furthermore, no CD19^{pos} cells escaped in CAR-STAb-T co-cultures even at the 1:16 E:T ratio, with only CD19^{neg}CD22^{pos} and double negative cells being able to escape immune control (figure 4b). There was no effective control for any of the different SEM cell variants from pooled CAR-T and TanCAR-T cell co-cultures at the lowest E:T ratios (figure 4b). Notably, the proliferation dynamics of the three SEM^{Luc} cell variants (SEM^{WT}, SEM-CD19^{KO} and SEM-CD22^{KO}) proved to be similar, as shown in online supplemental figure S4b.

Further in vitro experiments were performed to determine the dynamics of CD19 and CD22 surface expression downregulation in SEM cells that escape from T-cell control. SEM^{WT}, SEM-CD19^{KO} and SEM-CD22^{KO} were pre-stained with different cell trace dyes and a 33% SEM cell mix was co-cultured with the different effector T cells at the indicated E:T ratios for 4 days (figure 4c). CAR-STAb T cells were more effective than pooled CAR-T and TanCAR-T cells at all E:T ratios tested, and the enhanced cytotoxicity correlated with more effective control of CD19^{pos} and CD22^{pos} leukemia escape, especially at low

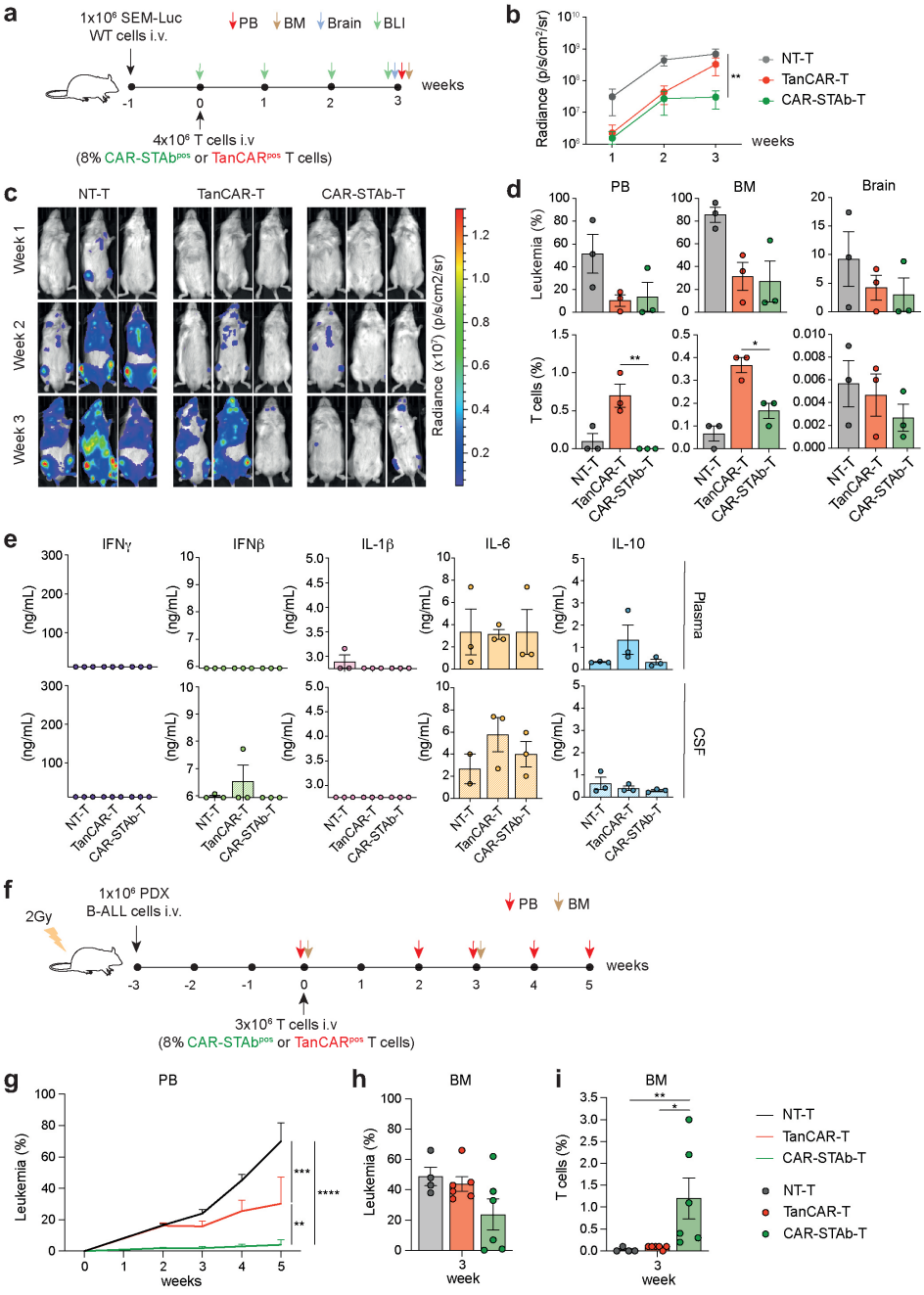

Figure 3 Comparative in vivo efficacy between CAR-STAb-T and TanCAR-T cells in tumor models co-expressing CD19 and CD22. (a) Experimental design of in vivo cytotoxicity in NSG mice receiving 1×10^6 SEM^{WT} cells, followed by intravenous injection of NT-T, CAR-STAb-T or TanCAR-T cells 4 days later. CAR-STAb^{pos} and TanCAR^{pos} cells, represented by GFP^{pos} cells, accounted for 8% of the total T cells injected. (b) Radiance quantification (photons s^{-1} cm^{-2} sr^{-1}) at the indicated time points. (c) Bioluminescence images showing disease progression from ventral view. (d) Leukemia progression and T-cell expansion measured by flow cytometry in peripheral blood, bone marrow and brain tissue at indicated time points. (e) Cytokine analysis in plasma and cerebrospinal fluid (CSF) samples from NSG mice treated with NT-T, TanCAR-T and CAR-STAb-T cells. IFN-γ, IFN-β, IL-1β, IL-6 and IL-10 were measured in a multiplex bead-based immunoassay. Results from (b,d,e) expressed as mean±SEM of three mice per group (n=3). (f) Experimental design of in vivo cytotoxicity in NSG mice receiving 1×10^6 primary B-ALL cells, followed by intravenous injection of NT-T, CAR-STAb-T or TanCAR-T cells 3 weeks later. CAR-STAb^{pos} and TanCAR^{pos} cells, accounted by GFP^{pos} cells, comprised 8% of the total injected T cells. (g,h) Percentage of leukemic cells measured by flow cytometry in peripheral blood (g) and bone marrow (h) at indicated time points. (i) Percentage of T cells measured by flow cytometry in bone marrow at week 3. Lines in (g) and bars in (h,i) represent mean±SEM of 4 mice for NT-T group and six mice for both CAR-STAb-T and TanCAR-T groups. (b,d,e,g–i) Statistical significance was calculated by two-way analysis of variance test corrected with a Tukey's test for multiple comparisons. B-ALL, B-cell acute lymphoblastic leukemia; BLI, bioluminescence signal; BM, bone marrow; CAR, chimeric antigen receptor; E:T, effector:target; IFN, interferon; IL, interleukin; i.v., intravenous; NT-T, non-transduced primary T cells; PB, peripheral blood; PDX, patient-derived xenograft; STAb, in situ secretion of T-cell redirecting bispecific antibodies; TanCAR, tandem CAR.

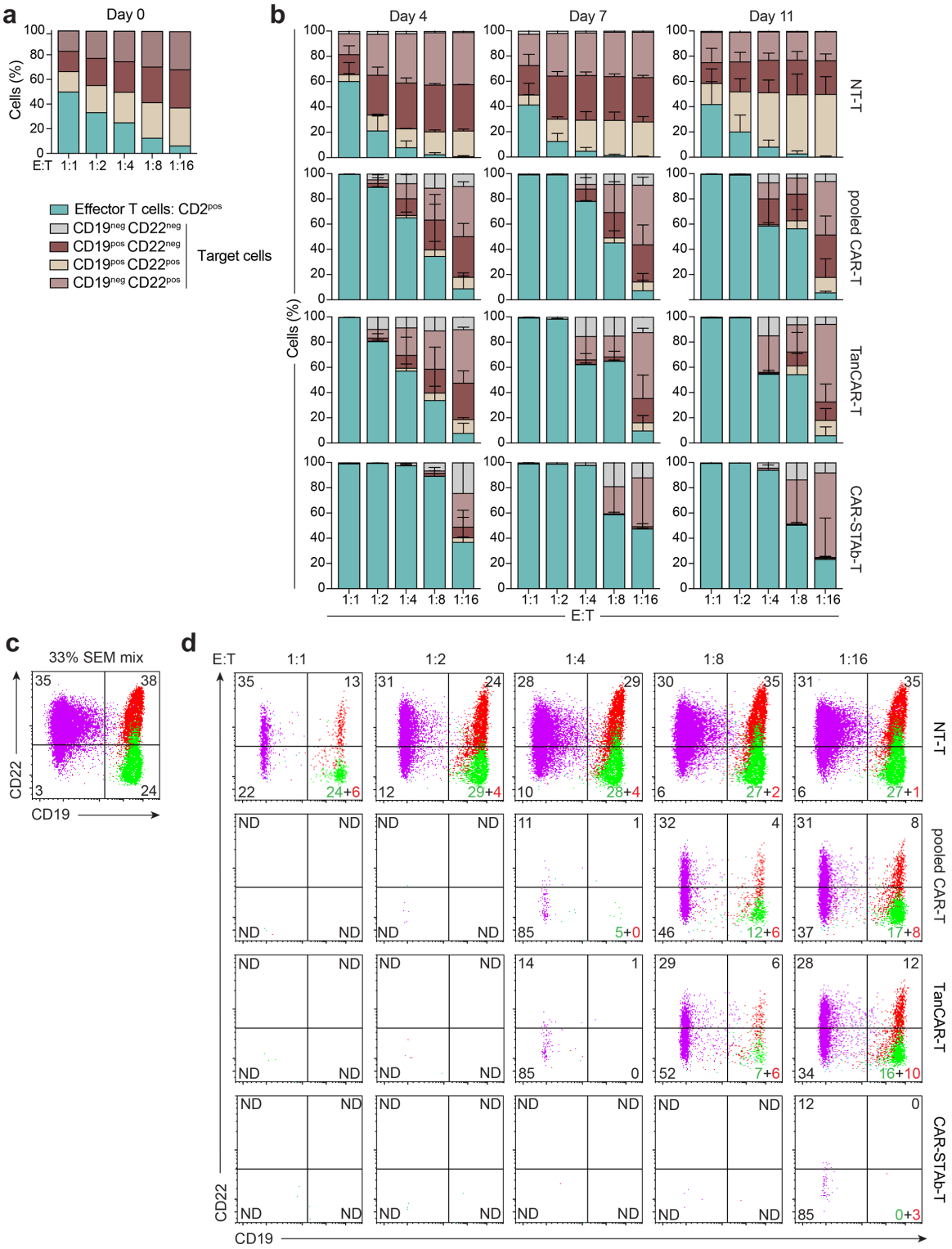

Figure 4 Cytotoxicity and leukemia control in vitro against heterogeneous tumors containing equal numbers of SEM^{WT}, SEM-CD19^{KO}, and SEM-CD22^{KO} cells (33% SEM cell mix). (a) NT-T, TanCAR-T, CAR-STAb-T or a 1:1 pool of CAR-19T and CAR-22T cells were co-cultured with the 33% SEM cell mix at the indicated ratios. (b) The expression of CD2, CD19 and CD22 was analyzed by flow cytometry after 4, 7 and 11 days to assess cytotoxic activity and leukemia escape over time. Data expressed as mean±SEM of two different experiments with independent donors (n=2). (c) CD19 and CD22 phenotype by flow cytometry at day 4 in a mix containing 33% of SEM^{WT}, SEM-CD19^{KO}, and SEM-CD22^{KO} cells after being stained at day 0 with CellTrace dyes (Far Red for SEM^{WT}, Violet for SEM-CD19^{KO} and CFSE for SEM-CD22^{KO}). (d) The stained 33% SEM cell mix was co-cultured with NT-T, TanCAR-T, CAR-STAb-T or a 1:1 pool of CAR-19T and CAR-22T cells at indicated effector:target ratios. After 4 days, CD19 and CD22 expression was determined by flow cytometry. Percentages of CD19^{neg}, CD22^{neg}, double negative and double positive cells are indicated. CAR, chimeric antigen receptor; NT-T, non-transduced primary T cells; STAb, in situ secretion of T-cell redirecting bispecific antibodies; TanCAR, tandem CAR.

E:T ratios (figure 4d). Only a small population of CD22^{neg} CD19^{KO}-derived SEM cells escaped CAR-STAb-T control at the 1:16 E:T ratio. In contrast, for dual-targeting CAR-based strategies, escape of CD19^{pos}, CD19^{neg} and double-positive cells was also evident at 1:8 and 1:16 E:T ratios (figure 4d). In both SEM-CD19^{KO} and double positive cells, a significant CAR-mediated downmodulation of CD22 was observed, being especially relevant at ratios 1:16 for CAR-STAb-T cells and 1:4 for TanCAR-T and pooled CAR-T cells (figure 4d).

CAR-STAb-T cells control heterogeneous leukemia more efficiently than dual-targeted CAR-T cells in vivo

To evaluate in vivo antitumor activity in a leukemia model with pre-existing CD19^{neg} and CD22^{neg} subpopulations, NSG mice were injected intravenously with 2.5×10^5 of the 33% SEM cell mix, followed 4 days later by intravenous injection of 5×10^6 NT-T, CAR-STAb-T, TanCAR-T or pooled CAR-T cells. Leukemia progression was followed weekly by BLI for 5 weeks or until the radiance humane endpoint of 2×10^7 photons was reached. PB and BM samples were analyzed by flow cytometry at the endpoint (figure 5a). Due to its aggressiveness, the leukemia developed rapidly in all mice, although tumor progression was attenuated in mice receiving pooled CAR-T, TanCAR-T or CAR-STAb-T cells compared with those receiving NT-T cells (figure 5b,c and online supplemental figure S10). In fact, only in two of all mice, both in the CAR-STAb-T group, radiance remained below the humane endpoint for the entire experiment, showing near complete leukemia remission at week 5 (figure 5b–d and online supplemental figure S10). Accordingly, analysis of PB and BM showed complete leukemia control in these two mice and increased T-cell expansion in the CAR-STAb-T-treated group (figure 5e). Although no differences in CD19^{pos} tumor escape were observed between the CAR-STAb-T, TanCAR-T, and pooled CAR-T groups in PB, further analysis in BM showed superior control of CD19^{pos} cells in CAR-STAb-T-treated mice compared with the TanCAR-T and pooled CAR-T groups (figure 5f). No differences in CD22^{pos} tumor control were observed between the three groups (figure 5f).

DISCUSSION

Despite recent advances in the treatment of R/R B-cell malignancies, a significant percentage of patients relapse following single-targeted T cell-redirecting CAR-T and TCE therapies, mainly due to immune pressure-mediated antigen loss.[8–10] Dual-targeted immunotherapies have been developed to prevent CD19 downmodulation and consequent tumor escape, some of which are already being tested in clinical trials.[22] Different multitargeting strategies have been designed, either using two independent CARs or assembling both binding domains into a single tandem CAR.[54 55] However, to date, the generation of dual-targeting CAR-T cell studies has not resulted in significantly improved outcomes compared with CD19 targeting alone.[23] Therefore, there is an urgent need to clarify which strategy could provide better disease control while avoiding the loss of tumor antigens.

Here, we report the first dual-targeted CAR-STAb-T strategy for B-ALL and compare it to previously validated dual-targeted CAR-based strategies, including a TanCAR-T cell therapy and the co-administration of a CD19/CD22 pooled CAR-T cell product.[21 31 56] T cells were engineered to express an anti-CD22 second-generation 4-1BB-based CAR and to secrete a CD19×CD3 TCE. Our group has extensively described one of the main mechanistic features of STAb-T cells compared with CAR-T cells, the ability to recruit bystander unmodified T cells.[36 37 39] Here, we demonstrated in both contact and non-contact co-culture systems with CD19^{pos} and/or CD22^{pos} cells that CAR-STAb-T cells efficiently redirected bystander T cells, resulting in enhanced cytotoxicity compared with that exhibited by TanCAR-T cells at low E:T ratios. In long-term in vitro co-culture assays, CAR-STAb-T cells also demonstrated better control of leukemia progression at low E:T ratios than TanCAR cells. Furthermore, this superior cytotoxic potential was not associated with an increased production of IFN-γ, thus reducing potential adverse events associated with cytokine release. In this regard, the different cytokine secretion profile observed between CAR-STAb-T and TanCAR-T cells, particularly with respect to TNF-α and IL-2 production, suggests divergent mechanisms of antitumor activity between CAR-T cells and TCEs. Specifically, our results indicate faster and more effective TCE-mediated tumor cell lysis in CAR-STAb-T cells and enhanced cellular expansion in TanCAR T cells, both mediated by the interaction with CD19. Although further experiments are needed to elucidate these mechanisms, the combination of CAR and STAb strategies may represent a promising approach to achieve both rapid and sustained antitumor responses in patients with advanced B-cell malignancies.

Regarding in vivo efficacy in CD19^{pos} CD22^{pos} cell-derived xenograft (CDX) and PDX models of B-ALL in a T-cell limiting experimental setting, CAR-STAb-T cells maintained a tighter control of tumor progression than TanCAR T cells, keeping the leukemia cell count almost undetectable. In terms of safety profile, systemic administration of TCEs has been frequently associated with cytokine release syndrome and immune effector cell-associated neurotoxicity syndrome.[57] Thus, the potential toxic effect caused by the sustained release of a TCE by engineered T cells may be a major concern for the translation of STAb-T therapies into the clinic. In this regard, we evaluated T-cell infiltration and cytokine release in the brain and CSF of mice treated with both CAR-STAb-T and TanCAR-T cells and found no differences between the two groups. In addition, TCE levels remained undetectable in plasma samples from CAR-STAb-T treated mice, consistent with the low levels of TCE observed in supernatants of primary CAR-STAb-T cells in vitro. As previously reported by others,[51] this observation may indicate that while CAR-STAb-T cells are primarily trafficked to tumor

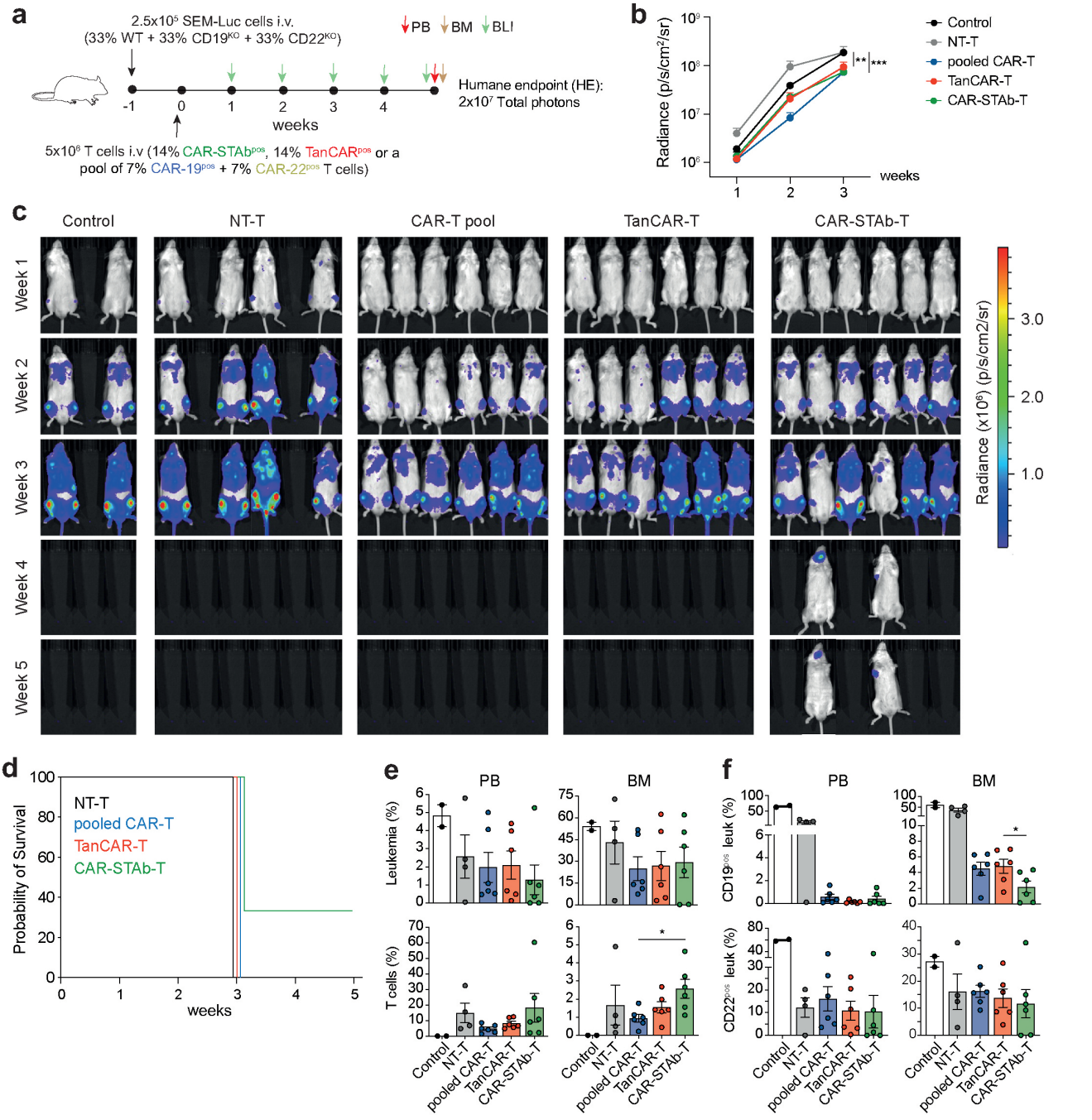

Figure 5 Comparative in vivo efficacy and tumor escape in a tumor model with heterogeneous expression of CD19 and CD22. (a) Experimental design of in vivo cytotoxicity in NSG mice receiving 2.5×10^5 33% SEM cell mix (SEM^{WT}, SEM-CD19^{KO}, and SEM-CD22^{KO} cells), followed by intravenous injection of NT-T, CAR-STAb-T, TanCAR-T or a 1:1 pool of CAR-19T and CAR-22T cells 4 days later. The percentage of transduced T cells, accounted by GFP^{pos} or tdTO^{os} cells, was equally adjusted for the different therapies and comprised 14% of the total T cells injected. (b) Radiance quantification (photons s^{-1} cm^{-2} sr^{-1}) at the indicated time points. A humane endpoint of 2×10^7 photons s^{-1} cm^{-2} sr^{-1} was established. (c) Bioluminescence images showing disease progression from ventral view. (d) Overall survival curve after 5 weeks of treatment. Mice were sacrificed according to the radiance humane endpoint of 2×10^7 photons s^{-1} cm^{-2} sr^{-1}. (e) Leukemia progression and T-cell expansion measured by flow cytometry in peripheral blood and bone marrow at endpoint. (f) CD19^{pos} and CD22^{pos} leukemia escape measured by flow cytometry in peripheral blood and bone marrow at endpoint. Percentages indicate CD19 or CD22 positive-stained cells gated from all HLA-ABC^{pos} CD3^{neg} cells. Data in (b,e,f) expressed as mean±SEM of 2 mice for the control group, four mice for the NT-T group and 6 mice for the CAR-STAb-T, TanCAR-T and pooled CAR-T groups. Each dot in (e,f) represents an independent mouse (n=2 for control group, n=4 for NT-T group and n=6 for CAR-STAb-T, pooled CAR-T and TanCAR-T groups). Statistical significance between groups was calculated either by two-way analysis of variance test corrected with a Tukey's test for multiple comparisons (b) or an unpaired Student's t-test (e,f). BLI, bioluminescence signal; BM, bone marrow; CAR, chimeric antigen receptor; i.v., intravenous; NT-T, non-transduced primary T cells; PB, peripheral blood; STAb, in situ secretion of T-cell redirecting bispecific antibodies; TanCAR, tandem CAR.

sites in the BM, where the bystander effect is mediated by locally delivered TCEs, the bispecific antibody is rapidly cleared from the PB and is therefore undetectable in the plasma.

Regarding escape mechanisms to CD19-targeted T cell-redirecting strategies, our previous work in B-ALL demonstrated that anti-CD19 STAb-T cells could prevent CD19 downregulation and subsequent tumor escape more efficiently than CD19-specific CAR-T cells.[36 38] Recent preclinical assays and clinical trials with dual CD19/CD22 targeting therapies have shown that $CD19^{neg}$ with persistent $CD22^{pos}$ is the predominant relapse phenotype, perhaps reflecting the poor performance of the CD22 CAR strategies,[23] but it is possible that the more variable and weaker expression of CD22 in leukemia cells[58] may be at the origin of the escape. The experiments conducted with cell lines and B-ALL CDX and PDX models have shown improved control of CD19, compared with CD22, tumor escape by CAR-STAb-T cells both in vitro and in vivo. In this context, using a heterogeneous target cell line model, CAR-STAb-T cells showed enhanced antitumoral activity in vitro against $CD19^{pos}CD22^{neg}$ and $CD19^{pos}CD22^{pos}$ cells when compared with TanCAR-T or pooled CD19/CD22 CAR-T cells, potentially reducing the risk of refractory $CD19^{pos}$ leukemia progression. However, due to the complex environment commonly associated with heterogeneous B-ALL, further experiments with different conditions and a larger number of mice should be performed to confirm the consistency of these results in vivo.

In this context, increased control over $CD19^{pos}$ tumor cells and the selection of an anti-CD22 scFv with the ability to recognize targets with low-antigen density may be crucial to avoid potential relapses. Although additional research is needed to fully assess the impact of antigen modulation on dual-targeted therapies, this aspect may be critical for the design and clinical implementation of more effective immunotherapies, such as a CAR-STAb-T cell combining CD19 CAR and CD22 TCE or a dual-targeted STAb-T strategy[59] based on T cells that secrete both CD19 and CD22 TCEs.

With an emerging pipeline of multitargeted therapies now being developed as an alternative to single-targeted CAR-T therapies, new concerns have been raised related to the appropriate recognition of all antigens, as well as those associated with production challenges. In this context, it is particularly relevant to determine whether these new strategies offer advantages over the dual infusion of single-targeting therapies beyond the regulatory and cost savings of producing a single product instead of two. Indeed, in this work, we demonstrate that the combination of a cell surface CD22 CAR and a soluble CD19 TCE may be advantageous over the use of conventional CD19/CD22 dual-targeted strategies based on cell surface anchored CARs, such as CD19/CD22 TanCAR-T cells, or a pool of single-targeted CD19 and CD22 CAR-T cells. Furthermore, we demonstrate that a small number of transduced CAR-STAb-T cells is sufficient to redirect non-transduced bystander T cells specifically and efficiently in the presence of leukemia cells, providing a significant advantage over current dual-target CAR-based adoptive T-cell therapies.

In summary, CAR-STAb-T cells could become an alternative to established dual-targeting CAR-T therapies for the treatment of R/R B-cell malignancies, especially in lymphodepleted patients with low T-cell counts, although future comprehensive comparative studies will be crucial as novel CAR-based multitargeting strategies emerge.

Author affiliations
[1]Cancer Immunotherapy Unit (UNICA), Department of Immunology, Hospital Universitario 12 de Octubre, Madrid, Spain
[2]Immuno-Oncology and Immunotherapy Group, Instituto de Investigación Sanitaria Hospital 12 de Octubre (imas12), Madrid, Spain
[3]H12O-CNIO Cancer Immunotherapy Clinical Research Unit, Spanish National Cancer Research Centre (CNIO), Madrid, Spain
[4]Josep Carreras Leukaemia Research Institute, Barcelona, Spain
[5]Red Española de Terapias Avanzadas (TERAV), Instituto de Salud Carlos III, Madrid, Spain
[6]Cancer Research Center (IBMCC, USAL-CSIC), Department of Medicine and Cytometry Service (NUCLEUS), University of Salamanca, Salamanca, Spain
[7]Biomedical Research Institute of Salamanca (IBSAL), Salamanca, Spain
[8]Centro de Investigación Biomédica en Red-Oncología (CIBERONC; CB16/12/00400), Instituto de Salud Carlos III, Madrid, Spain
[9]Spanish Network on Mastocytosis (REMA), Toledo and Salamanca, Spain
[10]Department of Immunology, Ophthalmology and ENT, School of Medicine, Universidad Complutense, Madrid, Spain
[11]Lymphocyte Immunobiology Group, Instituto de Investigación Sanitaria 12 de Octubre (i+12), Madrid, Spain
[12]Servicio de Inmunología, Hospital Clínic de Barcelona, Barcelona, Spain
[13]Institució Catalana de Recerca i Estudis Avançats (ICREA), Barcelona, Spain
[14]Department of Biomedicine, School of Medicine, Universitat de Barcelona, Barcelona, Spain
[15]Institut de Recerca Hospital Sant Joan de Déu–Pediatric Cancer Center Barcelona (SJD-PCCB), Barcelona, Spain
[16]CNIO-HMRIB Cancer Immunotherapy Clinical Research Unit, Spanish National Cancer Research Centre (CNIO), Hospital del Mar Research Institute Barcelona (HMRIB), Madrid/Barcelona, Spain
[17]Banc de Sang i Teixits (BST), Barcelona, Spain

X Javier Arroyo-Ródenas @jarroyo8, Clara Bueno @clarabueno_74, Pablo Menéndez @Menendez_Lab and Luis Álvarez-Vallina @Alvarez_Vallina

Acknowledgements We thank Dr Talía Velasco and Dr Narcis Fernández (Menendez's Lab) and Dr Victor M Diaz (OneChain Immunotherapeutics) for technical assistance. We thank the microcopy facility of the Universidad Complutense de Madrid.

Contributors Conception and design of the study: JA-R, CB, PM, LA-V. Acquisition of data: JA-R, AF, LDA, AM-M, HRH, FJG-E, AP-P, OA-S, MV-S, MG-R, BJ-M, G-MS, YP, CB-M. Analysis and interpretation of data: JA-R, LDA, OA-S, AR-F, AJ-R, EAG-N, MJ, BB, PR-N, AO, CB, PM, LA-V. Writing original draft: JA-R, LA-V. Review and editing: All authors. Guarantors: PM, LA-V.

Funding Research in LA-V laboratory is funded by the MCIN/AEI/10.13039/501100011033 (PID2023-148429OB-I00, PID2020-117323RB-I00, PDC2021-121711-I00, CPP2022-009762, CPP2022-009765, CPP2023-010827), the Carlos III (ISCIII) Health Institute with European Regional Development Fund (FEDER) cofinancing (DTS20/00089, PMPTA22/00167); the Asociación Española contra el Cáncer (AECC) (PROYE19084ALVA and PRYGN234844ALVA), the CRIS Cancer Foundation (FCRIS-2021-0090 and FCRIS-2023-0070), the Fundación "La Caixa" (HR21-00761 project IL7R_LungCan), the Fundación para la Investigación Biomédica del Hospital 12 de Octubre (programa Investiga 2022-0082), the Comunidad de Madrid (P2022/BMD-7225 Next Generation CART MAD), and the Fundación FERO (BBASELGAFERO2024.01). Research in PM/CB laboratory is supported by CERCA/Generalitat de Catalunya and Fundació Josep Carreras-Obra Social la Caixa for core support; "the European Research Council grants (ERC-PoC-957466 IT4B-TALL, ERC-PoC-101100665 BiTE-CAR); H2020

(101057250-CANCERNA), the MCIN/AEI/10.13039/501100011033 (PID2022-142966OB-I00 and Feder Funds), MCIN/European Union NextGeneration EU (CPP2021-008508 and CPP2022-009759); the AECC (PRYGN234975MENE and PRYGN211192BUEN), the Fundación Unoentrecienmil (FUECM2024), the ISCIII/FEDER (PI20/00822, PI24/00763) and the ISCIII-RICORS within the Next Generation EU program (plan de Recuperación, Transformación y Resilencia). BB is supported by the ISCIII (PI23/01256), AECC (INNOV211832BLAN) and Comunidad de Madrid (IND2022/BMD-23732). PR-N is funded by MCIN/AEI/10.13039/501100011033 (PID2020-115444GB-I00). AF was supported by a Juan de la Cierva fellowship from the Ministerio de Ciencia, Innovación y Universidades. LDA was supported by a Rio Hortega fellowship from the ISCIII (CM20/00004). OA-S was supported by a PhD fellowship from the Complutense University of Madrid. MG-R is supported by an Industrial PhD fellowship from Comunidad de Madrid (IND2022/BMD-23732).

Competing interests LA-V is a cofounder of Leadartis, a spin-off company focused on unrelated interests. LA-V and BB are cofounders of STAb Therapeutics, a spin-off company from the Research Institute Hospital 12 de Octubre (imas12). PM is cofounder of OneChain Immunotherapeutics, a spin-off company from the Josep Carreras Leukemia Research Institute.

Patient consent for publication Not applicable.

Ethics approval Human samples were obtained after written informed consent from the donors, and all studies were performed according to the principles expressed in the Declaration of Helsinki and approved by the Institutional Research Ethics Committees of the Hospitals and Research Centers involved in this study (HCB/2019/0450, HCB/2018/0030). The in vivo studies were carried out at the Barcelona Biomedical Research Park (PRBB) in accordance with the guidelines of the Animal Experimentation Ethics Committee in compliance with the institutional Animal Care Committee of the PRBB (DAAM11883).

Provenance and peer review Not commissioned; externally peer reviewed.

Data availability statement Data are available upon reasonable request.

ORCID iDs
Javier Arroyo-Ródenas http://orcid.org/0000-0003-1099-2018
Laura Díez-Alonso http://orcid.org/0000-0002-9545-6910
Beatriz Jiménez-Matías http://orcid.org/0009-0007-3217-6536
Manel Juan http://orcid.org/0000-0002-3064-1648
Luis Álvarez-Vallina http://orcid.org/0000-0003-3053-6757

REFERENCES

1 Westin JR, Kersten MJ, Salles G, *et al*. Efficacy and safety of CD19-directed CAR-T cell therapies in patients with relapsed/refractory aggressive B-cell lymphomas: Observations from the JULIET, ZUMA-1, and TRANSCEND trials. *Am J Hematol* 2021;96:1295–312.
2 Maude SL, Laetsch TW, Buechner J, *et al*. Tisagenlecleucel in Children and Young Adults with B-Cell Lymphoblastic Leukemia. *N Engl J Med* 2018;378:439–48.
3 Munshi NC, Anderson LD Jr, Shah N, *et al*. Idecabtagene Vicleucel in Relapsed and Refractory Multiple Myeloma. *N Engl J Med* 2021;384:705–16.
4 Neelapu SS, Locke FL, Bartlett NL, *et al*. Axicabtagene Ciloleucel CAR T-Cell Therapy in Refractory Large B-Cell Lymphoma. *N Engl J Med* 2017;377:2531–44.
5 Ortíz-Maldonado V, Rives S, Castellà M, *et al*. CART19-BE-01: A Multicenter Trial of ARI-0001 Cell Therapy in Patients with CD19$^+$ Relapsed/Refractory Malignancies. *Mol Ther* 2021;29:636–44.
6 Abramson JS, Palomba ML, Gordon LI, *et al*. Lisocabtagene maraleucel for patients with relapsed or refractory large B-cell lymphomas (TRANSCEND NHL 001): a multicentre seamless design study. *Lancet* 2020;396:839–52.
7 Kantarjian H, Stein A, Gökbuget N, *et al*. Blinatumomab versus Chemotherapy for Advanced Acute Lymphoblastic Leukemia. *N Engl J Med* 2017;376:836–47.
8 Shah NN, Fry TJ. Mechanisms of resistance to CAR T cell therapy. *Nat Rev Clin Oncol* 2019;16:372–85.
9 Yang X, Wei J, Zhou J. Overcoming resistance to anti-CD19 CAR T-cell therapy in B-cell malignancies. *Hematol Oncol* 2022;40:821–34.
10 Xu X, Sun Q, Liang X, *et al*. Mechanisms of Relapse After CD19 CAR T-Cell Therapy for Acute Lymphoblastic Leukemia and Its Prevention and Treatment Strategies. *Front Immunol* 2019;10:2664.
11 Locatelli F, Shah B, Thomas T, *et al*. Incidence of CD19-negative relapse after CD19-targeted immunotherapy in R/R BCP acute lymphoblastic leukemia: a review. *Leuk Lymphoma* 2023;64:1615–33.
12 Sotillo E, Barrett DM, Black KL, *et al*. Convergence of Acquired Mutations and Alternative Splicing of CD19 Enables Resistance to CART-19 Immunotherapy. *Cancer Discov* 2015;5:1282–95.
13 Jacoby E, Nguyen SM, Fountaine TJ, *et al*. CD19 CAR immune pressure induces B-precursor acute lymphoblastic leukaemia lineage switch exposing inherent leukaemic plasticity. *Nat Commun* 2016;7:12320.
14 Zhang Z, Chen X, Tian Y, *et al*. Point mutation in *CD19* facilitates immune escape of B cell lymphoma from CAR-T cell therapy. *J Immunother Cancer* 2020;8:e001150.
15 Rabilloud T, Potier D, Pankaew S, *et al*. Single-cell profiling identifies pre-existing CD19-negative subclones in a B-ALL patient with CD19-negative relapse after CAR-T therapy. *Nat Commun* 2021;12:865.
16 Bueno C, Barrera S, Bataller A, *et al*. CD34+CD19-CD22+ B-cell progenitors may underlie phenotypic escape in patients treated with CD19-directed therapies. *Blood* 2022;140:38–44.
17 Rosenthal J, Naqvi AS, Luo M, *et al*. Heterogeneity of surface CD19 and CD22 expression in B lymphoblastic leukemia. *Am J Hematol* 2018;93:E352–5.
18 Fry TJ, Shah NN, Orentas RJ, *et al*. CD22-targeted CAR T cells induce remission in B-ALL that is naive or resistant to CD19-targeted CAR immunotherapy. *Nat Med* 2018;24:20–8.
19 Baird JH, Frank MJ, Craig J, *et al*. CD22-directed CAR T-cell therapy induces complete remissions in CD19-directed CAR-refractory large B-cell lymphoma. *Blood* 2021;137:2321–5.
20 Qin H, Ramakrishna S, Nguyen S, *et al*. Preclinical Development of Bivalent Chimeric Antigen Receptors Targeting Both CD19 and CD22. *Mol Ther Oncolytics* 2018;11:127–37.
21 Zanetti SR, Velasco-Hernandez T, Gutierrez-Agüera F, *et al*. A novel and efficient tandem CD19- and CD22-directed CAR for B cell ALL. *Mol Ther* 2022;30:550–63.
22 Fergusson NJ, Adeel K, Kekre N, *et al*. A systematic review and meta-analysis of CD22 CAR T-cells alone or in combination with CD19 CAR T-cells. *Front Immunol* 2023;14:1178403.
23 de Oliveira Canedo G, Roddie C, Amrolia PJ. Dual-targeting CAR T cells for B-cell acute lymphoblastic leukemia and B-cell non-Hodgkin lymphoma. *Blood Adv* 2025;9:704–21.
24 Majzner RG, Mackall CL. Tumor Antigen Escape from CAR T-cell Therapy. *Cancer Discov* 2018;8:1219–26.
25 Shah NN, Maatman T, Hari P, *et al*. Multi Targeted CAR-T Cell Therapies for B-Cell Malignancies. *Front Oncol* 2019;9:146.
26 Blanco B, Compte M, Lykkemark S, *et al*. T Cell-Redirecting Strategies to “STAb” Tumors: Beyond CARs and Bispecific Antibodies. *Trends Immunol* 2019;40:243–57.
27 Haso W, Lee DW, Shah NN, *et al*. Anti-CD22-chimeric antigen receptors targeting B-cell precursor acute lymphoblastic leukemia. *Blood* 2013;121:1165–74.
28 Hudecek M, Sommermeyer D, Kosasih PL, *et al*. The nonsignaling extracellular spacer domain of chimeric antigen receptors is decisive for in vivo antitumor activity. *Cancer Immunol Res* 2015;3:125–35.
29 Guest RD, Hawkins RE, Kirillova N, *et al*. The role of extracellular spacer regions in the optimal design of chimeric immune receptors: evaluation of four different scFvs and antigens. *J Immunother* 2005;28:203–11.
30 James SE, Greenberg PD, Jensen MC, *et al*. Antigen sensitivity of CD22-specific chimeric TCR is modulated by target epitope distance from the cell membrane. *J Immunol* 2008;180:7028–38.
31 Velasco-Hernandez T, Zanetti SR, Roca-Ho H, *et al*. Efficient elimination of primary B-ALL cells in vitro and in vivo using a novel 4-1BB-based CAR targeting a membrane-distal CD22 epitope. *J Immunother Cancer* 2020;8:e000896.
32 De Munter S, Ingels J, Goetgeluk G, *et al*. Nanobody Based Dual Specific CARs. *Int J Mol Sci* 2018;19:403.

33 Blanco B, Ramírez-Fernández Á, Alvarez-Vallina L. Engineering Immune Cells for *in vivo* Secretion of Tumor-Specific T Cell-Redirecting Bispecific Antibodies. *Front Immunol* 2020;11:1792.
34 Aldoss I, Bargou RC, Nagorsen D, *et al*. Redirecting T cells to eradicate B-cell acute lymphoblastic leukemia: bispecific T-cell engagers and chimeric antigen receptors. *Leukemia* 2017;31:777–87.
35 Compte M, Cuesta AM, Sánchez-Martín D, *et al*. Tumor immunotherapy using gene-modified human mesenchymal stem cells loaded into synthetic extracellular matrix scaffolds. *Stem Cells* 2009;27:753–60.
36 Blanco B, Ramírez-Fernández Á, Bueno C, *et al*. Overcoming CAR-Mediated CD19 Downmodulation and Leukemia Relapse with T Lymphocytes Secreting Anti-CD19 T-cell Engagers. *Cancer Immunol Res* 2022;10:498–511.
37 Jiménez-Reinoso A, Tirado N, Martinez-Moreno A, *et al*. Efficient preclinical treatment of cortical T cell acute lymphoblastic leukemia with T lymphocytes secreting anti-CD1a T cell engagers. *J Immunother Cancer* 2022;10:e005333.
38 Ramírez-Fernández Á, Aguilar-Sopeña Ó, Díez-Alonso L, *et al*. Synapse topology and downmodulation events determine the functional outcome of anti-CD19 T cell-redirecting strategies. *Oncoimmunology* 2022;11:2054106.
39 Díez-Alonso L, Falgas A, Arroyo-Ródenas J, *et al*. Engineered T cells secreting anti-BCMA T cell engagers control multiple myeloma and promote immune memory in vivo. *Sci Transl Med* 2024;16:eadg7962.
40 Liu X, Barrett DM, Jiang S, *et al*. Improved anti-leukemia activities of adoptively transferred T cells expressing bispecific T-cell engager in mice. *Blood Cancer J* 2016;6:e430.
41 Velasquez MP, Bonifant CL, Gottschalk S. Redirecting T cells to hematological malignancies with bispecific antibodies. *Blood* 2018;131:30–8.
42 Al-Haideri M, Tondok SB, Safa SH, *et al*. CAR-T cell combination therapy: the next revolution in cancer treatment. *Cancer Cell Int* 2022;22:365.
43 Orlando EJ, Han X, Tribouley C, *et al*. Genetic mechanisms of target antigen loss in CAR19 therapy of acute lymphoblastic leukemia. *Nat Med* 2018;24:1504–6.
44 Choi BD, Yu X, Castano AP, *et al*. CAR-T cells secreting BiTEs circumvent antigen escape without detectable toxicity. *Nat Biotechnol* 2019;37:1049–58.
45 Yin Y, Rodriguez JL, Li N, *et al*. Locally secreted BiTEs complement CAR T cells by enhancing killing of antigen heterogeneous solid tumors. *Mol Ther* 2022;30:2537–53.
46 Cao G, Zhang G, Liu M, *et al*. GPC3-targeted CAR-T cells secreting B7H3-targeted BiTE exhibit potent cytotoxicity activity against hepatocellular carcinoma cell in the in vitro assay. *Biochem Biophys Rep* 2022;31:101324.
47 McGray AJR, Chiello JL, Tsuji T, *et al*. BiTE secretion by adoptively transferred stem-like T cells improves FRα+ ovarian cancer control. *J Immunother Cancer* 2023;11:e006863.
48 Huang S-W, Pan C-M, Lin Y-C, *et al*. BiTE-Secreting CAR-γδT as a Dual Targeting Strategy for the Treatment of Solid Tumors. *Adv Sci (Weinh)* 2023;10:2206856.
49 Román Alonso M, Grinyó-Escuer A, Duro-Sánchez S, *et al*. Generation of chimeric antigen receptor T cells targeting p95HER2 in solid tumors. *Nat Commun* 2024;15:9589.
50 Wehrli M, Guinn S, Birocchi F, *et al*. Mesothelin CAR T Cells Secreting Anti-FAP/Anti-CD3 Molecules Efficiently Target Pancreatic Adenocarcinoma and its Stroma. *Clin Cancer Res* 2024;30:1859–77.
51 Silva HJ, Martin G, Birocchi F, *et al*. CD70 CAR T cells secreting an anti-CD33/anti-CD3 dual-targeting antibody overcome antigen heterogeneity in AML. *Blood* 2025;145:720–31.
52 Yan Z, Gu R, Ma H, *et al*. A dual-targeting approach with anti-IL10R CAR-T cells engineered to release anti-CD33 bispecific antibody in enhancing killing effect on acute myeloid leukemia cells. *Cell Oncol (Dordr)* 2024;47:1879–95.
53 Kaur A, Shuken S, Yang AC, *et al*. A protocol for collection and infusion of cerebrospinal fluid in mice. *STAR Protoc* 2023;4:102015.
54 Guo Z, Tu S, Yu S, *et al*. Preclinical and clinical advances in dual-target chimeric antigen receptor therapy for hematological malignancies. *Cancer Sci* 2021;112:1357–68.
55 Marple AH, Bonifant CL, Shah NN. Improving CAR T-cells: The next generation. *Semin Hematol* 2020;57:115–21.
56 Castella M, Boronat A, Martín-Ibáñez R, *et al*. Development of a Novel Anti-CD19 Chimeric Antigen Receptor: A Paradigm for an Affordable CAR T Cell Production at Academic Institutions. *Mol Ther Methods Clin Dev* 2019;12:134–44.
57 Brudno JN, Kochenderfer JN. Current understanding and management of CAR T cell-associated toxicities. *Nat Rev Clin Oncol* 2024;21:501–21.
58 Lanza F, Maffini E, Rondoni M, *et al*. CD22 Expression in B-Cell Acute Lymphoblastic Leukemia: Biological Significance and Implications for Inotuzumab Therapy in Adults. *Cancers (Basel)* 2020;12:303.
59 Velasco-Sidro M, Arroyo-Ródenas J, Díez-Alonso L, *et al*. Dual-targeted STAb-T cells secreting BCMA and CD19 T cell engagers for improved control of haematological cancers. *Oncoimmunology* 2025;14:2444701.